Low-frequency Inductive Loop and Its Origin in the Impedance Spectrum of a Graphite Anode

Arun Thapa, Hongwei Gao

Low-frequency Inductive Loop and Its Origin in the Impedance Spectrum of a Graphite Anode

Arun Thapa and Hongwei Gao [z,]

Electrical & Computer Engineering Department, Montana State University, Bozeman, MT 59717, United States

Abstract

Graphite is a well-known anode material for commercial lithium-ion batteries, and its physical and electrochemical properties have been studied extensively. However, the origin of an inductive loop observed in the low-frequency region of the Nyquist complex plane impedance spectrum of the graphite anode has been widely debated and attributed to contrasting reasons. This paper investigates the impedance spectrum of the graphite anode at various states of charge (SoCs) using three-electrode galvanostatic Electrochemical Impedance Spectroscopy (EIS) and further explores the impedance response of the electrolyte as a function of frequency. The graphite anode EIS measurement displayed an inductive loop in the low-frequency region for almost entire SoCs, irrespective of the solid electrolyte interphase (SEI) age. To study the origin of this inductive loop in the graphite impedance spectrum, we fabricated a three-electrode pouch cell with graphite and NMC electrodes and estimated the electrolyte impedance in the frequency range from 1 MHz to 0.05 Hz. The electrolyte impedance at low frequencies exhibited inductive behavior, indicating a significant role of the electrolyte in the origin of the inductive characteristic in the low-frequency region of the graphite EIS spectrum.

Keywords:
Lithium-ion battery; Electrochemical Impedance Spectroscopy (EIS); Graphite; Electrolyte impedance; Three-electrode lithium-ion cell.

[z]**Corresponding author:** Tel: +1 (406) 994-5973
E-mail: hgao@ece.montana.edu (Hongwei Gao)

1. Introduction

In lithium-ion battery (LIB) research, Electrochemical Impedance Spectroscopy (EIS) is the most common technique to measure the impedance of an individual electrode or a cell under an applied sinusoidal voltage (potentiostatic EIS) or current (galvanostatic EIS) with a low amplitude over a wide frequency range. The measured impedance spectrum characterizes underlying electrochemical processes, such as charge carrier transfer kinetics and diffusion of active species occurring at the electrochemical double layers formed at the electrolyte/electrode interfaces and in the bulk interior of an electrode.[1] The most common practice for understanding the electrochemical processes and transport phenomena of a working electrode in a lithium-ion cell is to assemble a two-electrode cell with lithium as a counter/reference electrode and measure EIS under various conditions. In this context, the cell's impedance includes contributions of both the positive and negative electrodes, and it cannot be determined which electrode is responsible for each underlying physical phenomenon. This critical aspect has generally been ignored in published studies. Although impedance measurement of a series of symmetrical test cells with identical working electrodes and counter electrodes has been suggested to understand observed interfacial impedance changes in a single working electrode in a two-electrode cell[2], the complex and multistep process may not ensure the correct characterization of the electrochemical events occurring in the electrode. Therefore, it is suggested that EIS measurement using a three-electrode cell with a separate reference electrode is the most appropriate way to understand each electrode's electrochemical processes and transport phenomena.

Graphite is a well-known anode material for commercial LIBs with advantageous properties such as high electrical conductivity, a short path for ion diffusion, good electrolyte wettability, high theoretical lithium storage capacity, abundance, and low cost.[3] The solvent and lithium salt reduction during intercalation of lithium into the graphite electrode in the first few cycles produces a solid electrolyte interphase (SEI) layer on the electrode. It is commonly accepted that a robust and stable SEI layer is essential for the stability of the graphite electrode, ensuring its cyclability and long life. Various literature sources[2, 4-8] have reported the impedance measurement of the graphite anode using the three-electrode cell configuration with lithium as a reference electrode. Regarding the EIS of the graphite anode, an interesting feature that is frequently observed but not well understood is the presence of an inductive loop (the portion of an EIS spectrum where $-\mathrm{Im}(Z) < 0$) in the low-frequency region of the impedance spectrum,

which does not appear in the two-electrode EIS measurement. Despite various reports on the presence of inductive loops in EIS spectra of the graphite anodes, the origin of such loops has been widely debated and attributed to contrasting reasons.

The graphite anode forms a passivating film (SEI) during the first few charging/discharging cycles, and this SEI (specifically premature SEI) has been made responsible for the presence of an inductive loop in the EIS spectrum.[4] Gnanaraj et al.[4] observed inductive loops in low frequencies of the graphite anode impedance spectra and attributed the origin of such loops to the formation of the $Li_{1-X}C_6/C_6$ concentration cell with SEI separating the lithium-rich $Li_{1-X}C_6$ graphite and lithium-deficient C_6 graphite. The current flow during the discharge of the concentration cell opposes charging the graphite anode with lithium, creating an inductive loop. Zhuang et al.[9] used a similar approach to describe the inductive loops in the EIS spectra of the layered $LiCoO_2$ and spinel-type $LiMn_2O_4$ electrodes. It is essential to note that according to this concentration cell formation approach, the impedance spectrum of an electrode with a matured passivating film (after sufficient cycling) should not contain an inductive loop. Brandstätter et al.[5] examined the effect of the SEI on the electrical impedance response using two different electrode materials: graphite, well-known for SEI growth, and $Li_4Ti_5O_{12}$, known for almost negligible SEI growth. They found inductive loops in the impedance spectra of both anodes regardless of the types of the materials, SEI growth phenomena, and SEI ages.This finding contradicts the notion that the passivating layer, such as the SEI film, is responsible for the origin of the inductive behavior.

A few other reports have attributed the origin of the inductive loops to the electrode roughness and the Faradaic adsorption phenomenon at the electrode surfaces during the lithiation/delithiation processes.[2, 5, 10-12] However, none of these reports satisfactorily explain how adsorption without charge transfer leads to inductive behavior. Itagaki et al.[6] used a different approach to explain the low-frequency inductive loop. According to the report, the inter-layer distance of the graphene layers (sp^2 carbon atoms), which are weakly bonded by van der Waals force, increases due to lithium-ion intercalation. The increase in the inter-layer distance reduces the intercalation resistance for the following lithium ions during the intercalation process. Hence, the decrease in the reaction resistance at the intercalation sites produces the inductive loop in the impedance spectrum. Recently, inductive loops in both anode and cathode impedance spectra have been attributed to the lithium reference electrodes and their

positioning in the three-electrode cell configuration.[7, 13] The reference electrodes should not influence cell functioning and are merely there to help understand the characteristics of the working electrodes. Through a theoretical simulation, Hoshi et al.[13] predicted that the reference electrode creates a shortcut path for the current flow from the positive to the negative electrode, causing dissolution or corrosion of the reference electrode. They further suggested that the potential modulation caused by an inhomogeneous distribution of potential near the edges of the electrodes enhances the dissolution of the reference electrode, leading to the formation of inductive loops. These reports clearly show that the published literature does not provide satisfactory explanations for this important phenomenon in the graphite anode impedance spectra. Hence, the concept of the origin of the inductive loops in the low-frequency regions of the graphite EIS spectra needs to be revisited.

In order to investigate the origin of inductive loop formation in detail, in the present work, we assembled three-electrode lithium-ion cells using graphite anodes, lithium nickel manganese cobalt oxide ($LiNi_{0.3}Mn_{0.3}Co_{0.3}O_2$) cathodes, and lithium reference electrodes. We performed galvanostatic EIS measurements of the anodes, cathodes, and full cells at various states of charge (SoCs) in three-electrode cell configurations and compared the sum of cathode and anode EIS with the full cell EIS to confirm the proper functioning of the cells. Interestingly, graphite anode EIS spectra displayed inductive loops in the low-frequency regions for entire SoCs, irrespective of the SEI ages. Furthermore, we explored the impedance response of the electrolyte as a function of frequency using a three-electrode pouch cell. The electrolyte impedance exhibited inductive behavior in the low frequencies, which suggests that the electrolyte impedance contributes to the presence of the inductive loop in the anode impedance spectrum.

2. Experimental work

2.1 Cell assembly

In order to prepare electrodes for three-electrode cells, a commercial off-the-shelf LIB (Sony 18650VTC4, nominal capacity 2100 mAh) was discharged to 2.5 V at C/5 current rate as the preparation for the battery opening procedure. The fully discharged battery was disassembled inside a glovebox, as shown in Figure 1a. The anode (graphite coated on copper current collector) and cathode ($LiNi_{0.3}Mn_{0.3}Co_{0.3}O_2$ coated on the aluminum current collector, commonly known as NMC) were carefully separated and cleaned immediately with dimethyl carbonate

(DMC) to remove the electrolyte. Then, the electrodes were left to dry for 24 hours inside the globe box to eliminate the residual electrolyte and phosphates from the electrode surfaces. The active material on one side of each electrode was removed using N-Methyl-2-Pyrrolidone (NMP) as the electrodes of the commercial battery were coated with active materials on both sides. Then, the anode and cathode disks with a diameter of 14 mm were punched out inside the glovebox. The three-electrode lithium-ion cells were assembled inside the argon-filled glove box in moisture and oxygen-controlled conditions (H_2O < 0.5 ppm and O_2 < 0.1 ppm). MTI split cell kits were used to assemble the three-electrode cells, as shown in Figure 1b. A lithium ring (99.9 %, Sigma-Aldrich) with an outer and inner diameter of 26 mm and 20 mm, respectively, was used as the reference electrode in each of the three-electrode cells, as shown in Figure 1c. The anode, reference electrode, and cathode were separated electronically using polypropylene films (Celgard® H2013, thickness 20 µm, PP|PE|PP), while 1 M lithium hexafluorophosphate ($LiPF_6$) dissolved in a mixture of ethylene carbonate (EC) and dimethyl carbonate (DMC) (v/v = 1:1) (Sigma-Aldrich) was used as the electrolyte.

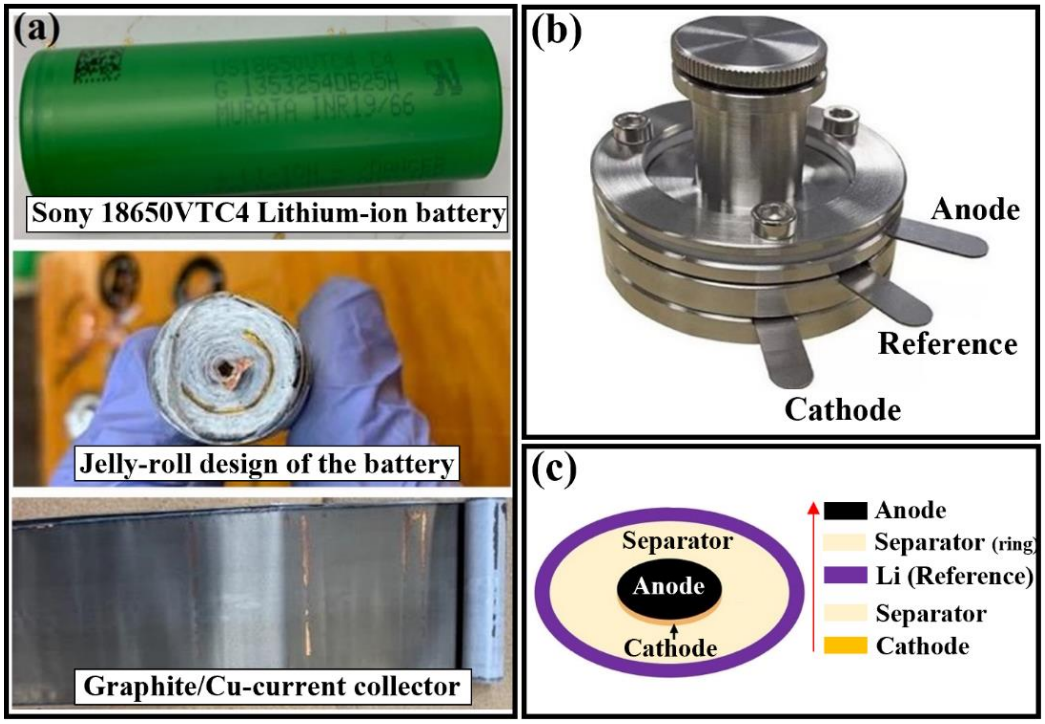

Figure 1. (a) As-received commercial Sony 18650VTC4 lithium-ion battery showing the jelly-roll design and graphite/Cu anode after disassembly of the battery inside the glovebox. (b) MTI three-electrode split cell kit. (c) Schematic showing the arrangement of the cell components inside the three-electrode lithium-ion test cell.

In addition, a three-electrode pouch cell was assembled to study the electrolyte impedance, as shown in Figure 2. Two identical NMC electrodes (2 cm × 5.5 cm) were placed on either side of a graphite electrode (2 cm × 5.5 cm). A distance of 1 cm from the first NMC electrode (denoted as electrode #1) to the graphite electrode (denoted as electrode #2) was maintained, while electrode #2 was 3 cm apart from the second NMC electrode (denoted as electrode #3). No separator was used in the assembly, and a 3 mL electrolyte was used in the pouch cell. The pouch cell was rested for 24 hours for electrolyte wetting before performing the EIS tests.

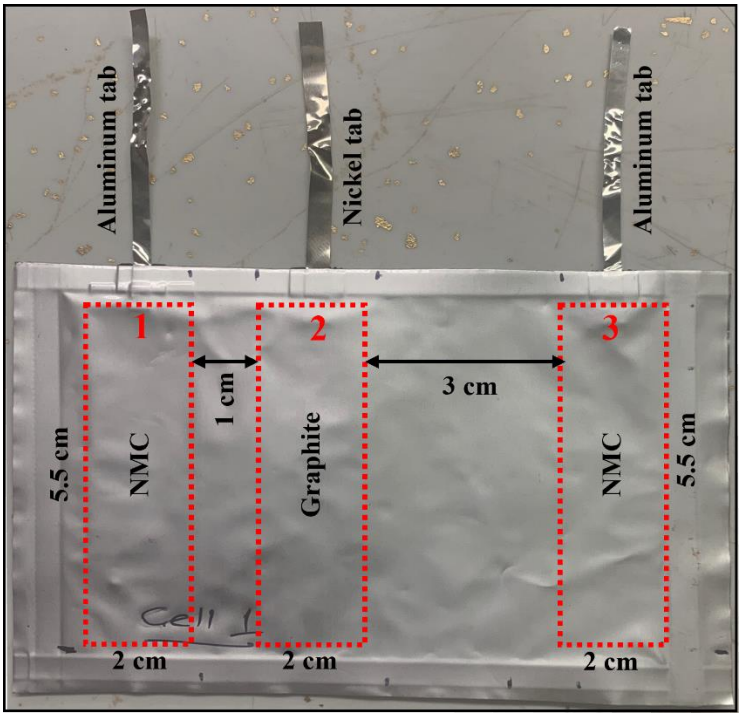

Figure 2. Photograph of a three-electrode pouch cell used for measuring the EIS of the electrolyte.

2.2 EIS measurement

Before performing the EIS tests, all the cells, except the pouch cell, were subjected to five initialization cycles (full cell, CC-CV charging with C/5 rate, CC discharging with C/5 rate, and a 5 min rest between charging and discharging) with cut-off potentials at 2.5 V and 4.2 V at ambient temperature using an LBT21084HC Arbin cycler to ensure stable cell performance, determine the cell capacities and set a well-defined state of charge (SoC). The EIS tests were performed in the galvanostatic mode, a recommended mode for a low-impedance electrochemical system such as lithium-ion cells, using a Gamry Reference 3000 potentiostat/galvanostat. In order to perform the EIS measurement as the SoC decreases, cells were fully charged first and then discharged at the C/5 rate in steps of various decreasing SoCs at

which the open circuit potential and impedance were measured. On the other hand, to measure the EIS as the SoC increases, cells were fully discharged first and charged in steps of various SoCs where the open circuit potential and impedance were measured. Cells were rested for three hours before measuring impedance in order to let open circuit potential stabilize. The alternating current amplitude was set to 5% of the cell capacity to ensure linearity and a good signal-to-noise ratio. Unless otherwise stated, the cell impedance was measured in the frequency range between 100 kHz and 0.05 Hz in an automatic sweep mode from high to low frequency, and all measurement was carried out at room temperature. The reproducibility and reliability of the cell assembly procedure and impedance measurement were assessed for different cells.

3. Results and discussion

Accurate EIS measurement of energy conversion and storage devices such as LIBs having very low impedances is challenging. One of the problems encountered in measuring the EIS of such devices is the inductive effect originating from the connecting leads of the instrument, typically in the high-frequency region. Such an inductive effect has been reported for large-capacity commercial LIBs rather than small-capacity ones.[2, 14] To minimize the measurement errors, the ground impedance of the instrument, the so-called "cable-short impedance," was measured, as shown in Figure 3a. The Nyquist complex plane impedance plot shows the inductive effect of the connecting leads. However, the minimal (~150 mΩ) connecting lead resistance should not affect measured EIS data in this work. Furthermore, it is essential to determine an appropriate cell rest period after charging/discharging to a certain SoC and before measuring the EIS to ensure that the cell is electrochemically stable. Otherwise, the electrochemically unstable cell can create drift issues during the impedance measurement, producing artifacts in the impedance spectrum. Therefore, the EIS measurement was taken using a three-electrode setup (see Figure 1) after 3 hours and 12 hours of rest after charging the cell to 80% SoC, as shown in Figure 3b. The figure shows two almost overlapping impedance spectra measured after 3 and 12 hours, confirming cells' chemical stability after 3 hours of rest.

A general practice to study the kinetic and mass transport properties at the interfacial region of the working electrode is to assemble a two-electrode cell in a half-cell configuration with lithium as a counter/reference electrode. Nevertheless, it should be noted that the impedance spectrum of the half-cell includes the interfacial properties of both the working and counter

electrodes. It does not precisely represent the impedance characteristic of the working electrode alone.[2, 5] Therefore, anode impedance measurement in a three-electrode configuration has been conducted in this work.

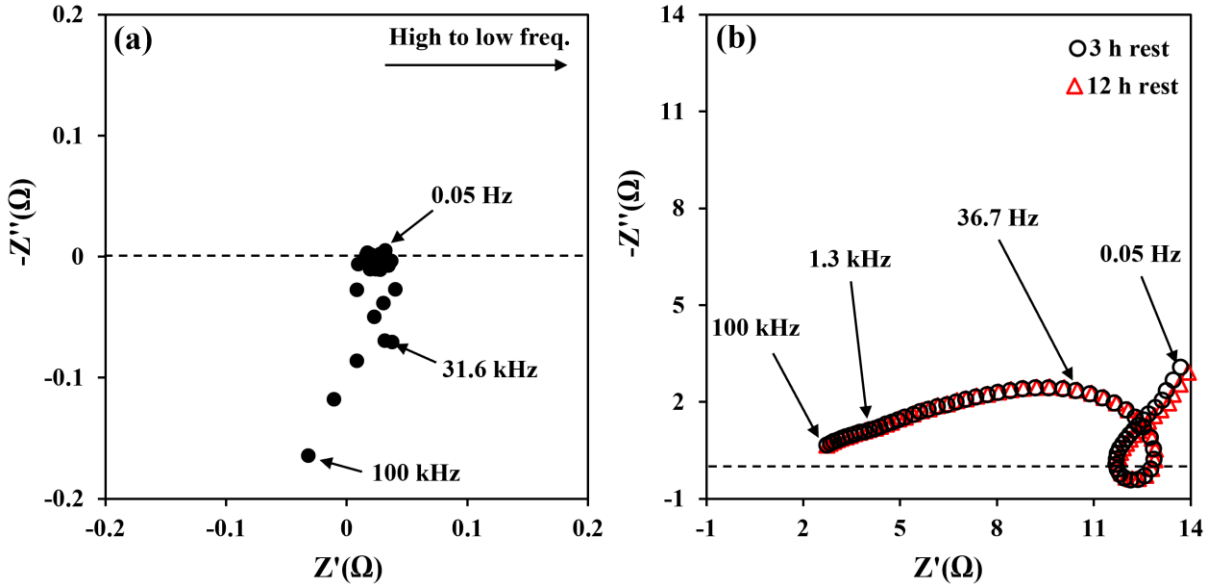

Figure 3. (a) Cable-short impedance spectrum of the instrument. (b) Comparison of anode impedance spectra measured after different rest periods. The anode impedance measurements were performed using a three-electrode setup, as shown in Figure 1.

Three-electrode lithium-ion cells were assembled with working electrodes of graphite (anode) and NMC (cathode) and reference electrodes of lithium rings, as shown in Figure 1 and as described in Section 2.1. Figure 4a displays the complex plane plot of the graphite anode impedance spectra measured at decreasing SoC steps. Each impedance spectrum of the graphite anode comprises a small semicircle followed by a bigger semicircle above the real axis (Z' axis) and one below the real axis, the so-called "inductive loop." The spectrum also shows an inclined line to the Z' axis at low frequencies in all SoCs. The first semicircle with a small diameter is located at high frequencies above 10 kHz, the second semicircle, which shows the highest impedance contribution, is located at medium frequencies between 10 kHz and 6.5 Hz, and the inductive loop occurs at low frequencies between 6.5 Hz and 0.32 Hz depending on the SoC. The size of the high-frequency semicircle is not changed over the entire SoCs. In contrast, the size of the medium-frequency semicircle increases with a decrease in the SoC. Furthermore, the size of the inductive loop remains almost similar for the entire SoC range except for the 20% SoC. The data shown within a circle (green color) in the Bode plot, as shown in Figure S1a, correspond to the inductive loop in the Nyquist plot of the graphite anode EIS which shows positive phase

angles for several data points. A detailed explanation of the cathode and full cell impedances is outside the scope of this work and hence is not discussed here.

In order to verify the cell functioning and to examine the full cell impedance variation per anode and cathode impedance, the anode and cathode impedance were added and compared with the measured full cell impedance. One typical example is shown in Figure 4b, which shows that the measured full cell impedance overlaps very well with the one obtained after adding anode and cathode impedance. Figure 4c shows equivalent circuit models (ECMs) for fitting the anode, cathode, and full cell impedance spectra, where R_s is a pure resistor, R_{SEI} and CPE_{SEI} are a

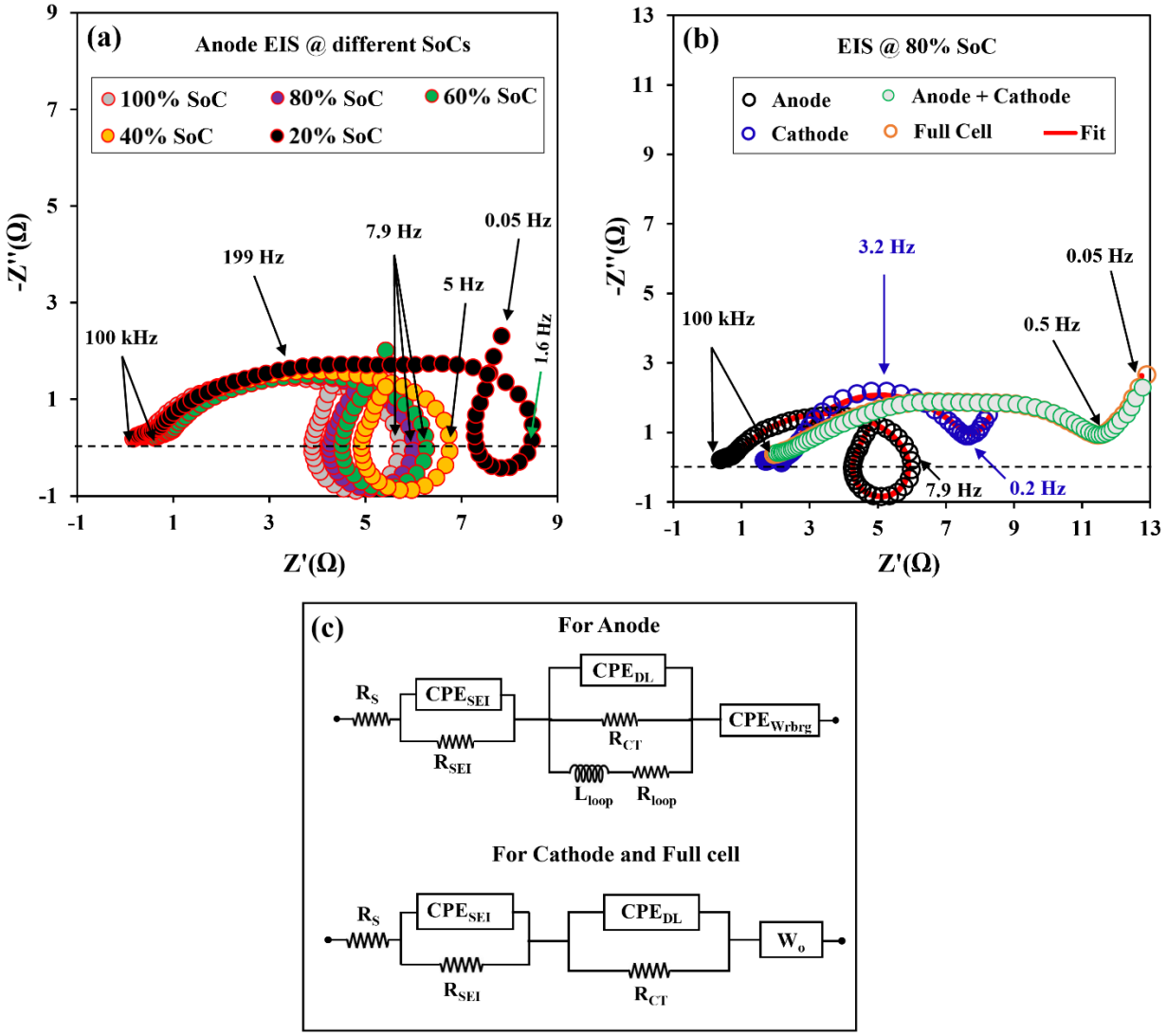

Figure 4. (a) Impedance spectra of the graphite anode measured at decreasing SoC steps. (b) Impedance spectra of the anode, cathode, and full cell at 80% SoC. (c) Equivalent circuit models (ECMs) to fit the impedance spectra. The anode, cathode, and full cell impedance measurements were performed using a three-electrode setup, as shown in Figure 1.

resistor and a constant phase element for modeling the SEI, $R_{CT,}$ and CPE_{DL} are a resistor and a constant phase element for modeling the charge transfer layer, L_{loop} and R_{loop} are an inductor and a resistor for modeling the inductive behavior of the anode spectrum along with other elements in the ECM, and W_0 and CPE_{wrbrg} are a Warburg impedance and a constant phase element modeling the Warburg impedance. CPEs are commonly used for electrodes with inhomogeneous surface morphology (such as carbon electrodes or polycrystalline metal surfaces) and varying thickness or composition of active materials coating.[15] The following equation can be used to calculate the capacitance of an equivalent circuit for a parallel combination of a CPE and a resistor (R).[16]

$$C = \frac{(R.Q)^{1/\alpha}}{R}$$

where Q is the CPE element and α is an empirical constant (or power factor) representing how close the CPE's behavior is to a resistor (α = 0) or a pure capacitor (α = 1).

In the case of the anode EIS spectrum, the intercept at the Z' axis at high frequency corresponds to the equivalent serial resistance (R_s), which relates to the total resistance of the electrolyte, separator, and electrical contacts. The number of resistor-CPE networks depends on the number of distinctive semicircles in the impedance spectrum. The first resistor-CPE network represents the high-frequency semicircle related to the passivated film (SEI) impedance on the anode surface (R_{SEI}) and the second resistor-CPE network corresponds to the semicircle at a high- to medium-frequency region above the real axis (Z' axis) which can be ascribed to the charge transfer resistance (R_{CT}).[17-19] In addition, a series network of a resistor (R_{loop}) and an inductor (L_{loop}), connected with CPE_{DL} and R_{CT} in a parallel network, represents the inductive loop present in the low-frequency region of the anode impedance spectrum. The straight-line inclined to the Z' axis in the low-frequency region of the anode EIS spectrum represents the Warburg region, which can be attributed to the lithium diffusion process within the graphite anode. In this work, a constant phase element (CPE_{Wrbrg}) was used to fit the Warburg impedance. A similar ECM has been used to fit an anode EIS spectrum with an inductive loop by Itagaki et al.[20] Figure 4b shows that ECMs fit measured impedance spectra very well, which is further verified by Bode plots shown in Figure S1a-c. The parameters obtained after fitting the experimental curve (anode impedance spectrum at 80% SoC) by the ECM are presented in Table 1. It should be noted that the validity of the EIS spectra was checked by analyzing their

reproducibility by the Kramers-Kronig (K-K) compliant equivalent circuit before performing any ECM fit.[21, 22]

Furthermore, the EIS spectra of the graphite anode were also measured at various increasing SoC steps during the charging process, which further confirmed the existence of inductive loops in the low-frequency regions of the anode impedance spectra (data not shown in this manuscript). A few reports have suggested that the inductive loop, in the case of the graphite anode EIS spectrum, is due to the immature SEI formation (leaky SEI) during the first formation cycle and should not be present for matured SEI (i.e., after a sufficient number of charge/discharge cycles).[4, 9] To examine the notion that the electrode with a matured passivating layer should not show an inductive loop in the EIS spectrum, we recorded the graphite anode impedance after 100 charge/discharge cycles (data not shown in this manuscript) which showed the inductive loop even after long charge/discharge cycles. This outcome is consistent with those demonstrated in literature[2, 5, 12]. In addition, Brandstätter et al.[5] observed inductive loops for different materials known for good SEI growth and almost negligible SEI growth. This outcome indicates that the passivating layer (e.g., SEI) can not be responsible for the origin of the inductive behavior. Although the electrode's roughness and the Faradaic adsorption phenomenon at the electrode's surface during the lithiation/delithiation process have been considered as possible reasons for an inductive loop[10-12], none of these reports satisfactorily explain how adsorption without charge transfer leads to inductive behavior. These results show that the electrode can not be responsible for the inductive behavior in the graphite anode EIS spectrum.

Table 1. Values of the circuit components obtained after fitting the experimental curve (graphite anode impedance spectrum at 80% SoC) by the equivalent circuit shown in Figure 4c.

Component	Description	Values	Error
R_s	Series resistance	0.12 Ω	-
R_{SEI}	Surface film (SEI) resistance	0.51 Ω	0.1×10^{-1} Ω
Q_{SEI}	CPE element for surface film	4.77×10^{-4} Ss^{α}	2.5×10^{-5} Ss^{α}
α_{SEI}	Empirical constant for surface film	0.63	3.9×10^{-2}
R_{CT}	Charge transfer resistance	5.88 Ω	0.1 Ω
Q_{DL}	CPE element for double layer	2.72×10^{-3} Ss^{α}	2.6×10^{-4} Ss^{α}
α_{DL}	Empirical constant for double layer	0.62	1.1×10^{-2}
R_{loop}	Inductive loop resistance	8.29 Ω	7.3×10^{-1} Ω

L_{loop}	Inductive loop inductance	0.99 H	8.6×10^{-2} H
Q_{Wrbrg}	CPE element for Warburg impedance	1.89 Ss^{α}	0.3 Ss^{α}
α_{Wrbrg}	Empirical constant for Warburg impedance	0.67	0.1
χ^2	Goodness of fit	4.67×10^{-4}	

The existing explanation of the origin of the inductive loop at low frequencies of the graphite anode impedance is solely based on the electrode morphology and electrode/electrolyte interface (passivation layer). The electrolyte impedance, in general, is considered purely resistive ($Z_{electrolyte} = R_s$). However, the inductive nature of the electrolyte has already been explored and explained in terms of an opposing force that can be generated by frictions resulting from the ion atmosphere relaxation effect and the electrophoretic effect.[23-25] Hence, it is noteworthy to consider the inductive property of the electrolyte regarding the occurrence of an inductive loop in the graphite anode impedance spectrum. That means the frequency-dependent electrolyte impedance should be expressed as $Z_{electrolyte} = R_s + j2\pi f L_{electrolyte}$, where j, f, and $L_{electrolyte}$ represent the imaginary unit number, frequency, and electrolyte inductance, respectively. To explore the frequency-dependent impedance response of the electrolyte, we fabricated a three-electrode pouch cell with graphite and NMC electrodes, as shown in Figure 2 and as described

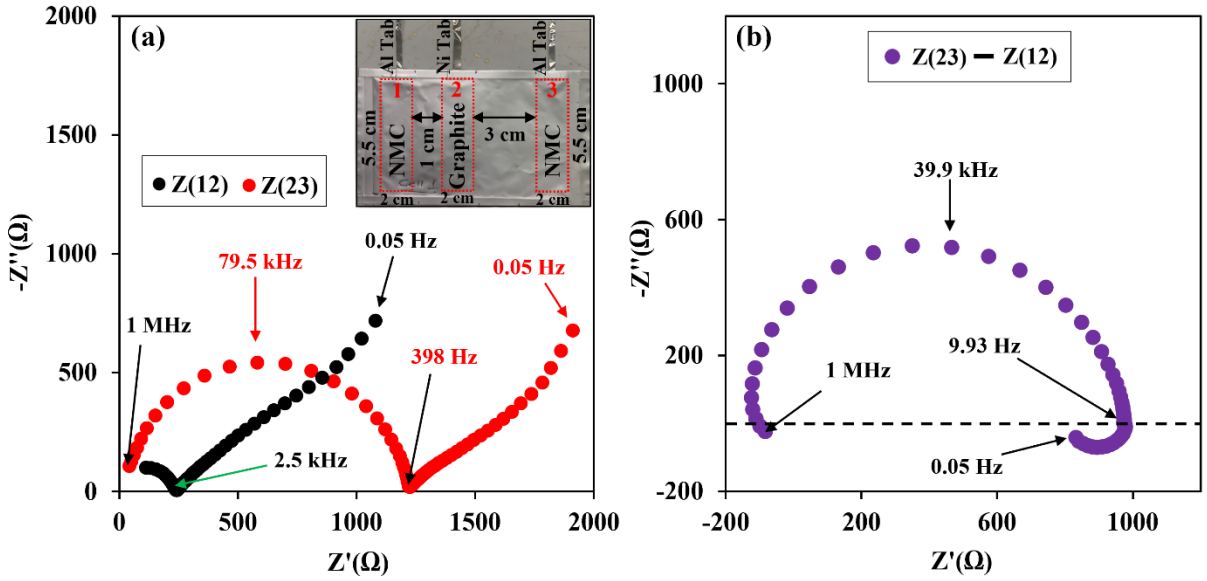

Figure 5. Impedance measurement of the three-electrode pouch cell. (a) Nyquist plots of the EIS spectra measured between electrodes #1 and #2, i.e., Z(12), and between electrodes #2 and #3, i.e., Z(23). (b) A Nyquist plot of the impedance spectra obtained after series subtraction from Z(23) to Z(12). The inset in Figure 5a represents a photograph of a three-electrode pouch cell used for measuring the EIS of the electrolyte.

in Section 2.1. The galvanostatic EIS spectra were measured between NMC and graphite electrodes at a short distance, i.e., Z(12), and a long distance, i.e., Z(23), in the frequency range of 1 MHz and 0.05 Hz, as shown in Figures 5a. Both EIS spectra exhibit a semicircle in the high to medium-frequency range above the real axis (Z' axis) and a straight line inclined at ~45° angle to the Z' axis in the medium to low-frequency region. The semicircles in the EIS spectra can be ascribed to the charge transfer resistance, whereas the straight lines can be attributed to the lithium diffusion processes within the electrodes.

The overall impedance measured between electrodes at a longer distance is higher than that at a shorter distance which can also be seen in Bode plots shown in Figure S2a. Also, the phase angles for Z(12) and Z(23) show negative values for the entire frequency range, indicating no inductive behavior in the impedance spectra. In order to estimate the electrolyte impedance, we performed a series subtraction between impedances Z(12) and Z(23) in the same frequency range mentioned above, as shown in Figure 5b. Z(12) is considered as the sum of the impedance of electrode #1 (the first NMC electrode), the impedance of electrode #2 (the graphite electrode), and the impedance of the electrolyte between electrode #1 and electrode #2. In contrast, Z(23) is considered as the sum of the impedance of electrode #3 (the second NMC electrode), the impedance of electrode #2 (the graphite electrode), and the impedance of the electrolyte between electrode #3 and electrode #2. Since the material and dimension of the two NMC electrodes are the same, their impedances are considered the same. As a result, the subtraction between Z(12) and Z(23) cancels the impedances of the electrodes. Only the difference between the impedances of the electrolytes, i.e., the electrolyte between electrode #1 and electrode #2 and the electrolyte between electrode #3 and electrode #2, remains. If the impedances of the electrolytes are considered to be proportional to the width of the electrolyte bodies (1 cm and 3 cm, as shown in Figure 2), the difference between Z(12) and Z(23) should correspond to the impedance of an electrolyte body whose width is 2cm (3cm-1cm). Interestingly, as shown in Figure 5b, the impedance spectrum shows inductive behavior in the region of our interest, i.e., in the low-frequency region. The Bode plot, shown in Figure S2b, further confirmed the inductive behavior of the electrolyte impedance spectrum as the phase angles show positive values (points with green color) for low frequencies. This result indicates that the inductive behavior of the electrolyte has an important role in the origin of the inductive loop in the low-frequency region of the graphite EIS spectrum.

Some published reports[26, 27] have shown no inductive loops in the EIS spectra of the graphite anodes, while our work shows inductive loops in the low-frequency regions of the graphite anode EIS spectra. Moreover, our work shows that electrolyte plays an important role in the origin of inductive behavior in the EIS spectrum. However, this inductive behavior may not result from the electrolyte alone. The electrolyte transport resistance coupled with other kinetics and solid-state diffusion processes in the electrodes and electrode/electrolyte interfaces could collectively cause inductance. Since the kinetics and solid-state diffusion processes can be different in different cell assemblies and configurations, the cell assembly and configuration can play an important role in the presence of the inductive loop and, generally, EIS measurements and analysis.

4. Conclusions

In summary, this work aimed to study the origin of the inductive loop in the Nyquist complex plane impedance plot of the graphite anode. For this purpose, we assembled three-electrode lithium-ion cells and measured the galvanostatic EIS of the graphite anode at various states of charge (SoCs). To ensure proper cell functioning, we compared the sum of the cathode and anode EIS with the full cell EIS in the same frequency range. The experimental EIS for full cell closely agreed with the sum of the cathode and anode EIS spectra. The graphite anode EIS spectra measured in the three-electrode configuration displayed inductive behavior in the low-frequency regions for the entire SoCs. In order to study the origin of this inductive behavior in the low-frequency region of the graphite anode EIS spectrum, we fabricated a three-electrode pouch cell with graphite and NMC electrodes. With the help of the three-electrode pouch cell, we estimated the electrolyte impedance in the frequency range of 1 MHz and 0.05 Hz. The electrolyte impedance at low frequencies exhibited inductive behavior, indicating a significant role of the electrolyte in the origin of the inductive characteristic in the low-frequency region of the graphite EIS spectrum. However, it may not be the electrolyte alone that causes the inductive behavior; rather, the electrolyte impedance, charge transport kinetics, and solid-state diffusion processes in the cells may collectively cause the inductive behavior. Since the kinetics and diffusion processes can be different in different cell assemblies or configurations, the cell assembly and configuration are important for the origin of the inductive behavior, and in general, for EIS measurement and analysis.

CRediT authorship contribution statement

Arun Thapa: Conceptualization, Methodology, Investigation, Formal analysis, Writing - original draft. **Hongwei Gao:** Conceptualization, Methodology, Discussion, Formal analysis, Validation, Funding acquisition, Review & editing.

Conflict of interest

The authors declare no conflict of interest.

Acknowledgment

Research was sponsored by the DEVCOM Army Research Laboratory (ARL) and was funded under Cooperative Agreement (CA) Number W911NF-20-2-0284. The views and conclusions contained in this document are those of the authors and should not be interpreted as representing the official policies, either expressed or implied, of the DEVCOM Army Research Laboratory or the U.S. Government. The U.S. Government is authorized to reproduce and distribute reprints for Government purposes notwithstanding any copyright notation hereon.

References

1. N. Meddings, M. Heinrich, F. Overney, J.-S. Lee, V. Ruiz, E. Napolitano, S. Seitz, G. Hinds, R. Raccichini, and M. Gaberšček, *Journal of Power Sources*, **480** 228742 (2020).
2. J. Song, H. Lee, Y. Wang, and C. Wan, *Journal of Power Sources*, **111** (2), 255-267 (2002).
3. H. Zhang, Y. Yang, D. Ren, L. Wang, and X. He, *Energy Storage Materials*, **36** 147-170 (2021).
4. J. Gnanaraj, R. W. Thompson, S. Iaconatti, J. DiCarlo, and K. Abraham, *Electrochemical and Solid State Letters*, **8** (2), A128 (2005).
5. H. Brandstätter, I. Hanzu, and M. Wilkening, *Electrochimica acta*, **207** 218-223 (2016).
6. M. Itagaki, N. Kobari, S. Yotsuda, K. Watanabe, S. Kinoshita, and M. Ue, *Journal of Power Sources*, **135** (1-2), 255-261 (2004).
7. S. J. An, J. Li, C. Daniel, S. Kalnaus, and D. L. Wood, *Journal of the Electrochemical Society*, **164** (7), A1755 (2017).
8. J. Huang, H. Ge, Z. Li, and J. Zhang, *Electrochimica Acta*, **176** 311-320 (2015).
9. Q.-C. Zhuang, X.-Y. Qiu, S.-D. Xu, Y.-H. Qiang, and S. Su, *Lithium Ion Batteries—New Developments*, **8** 189-227 (2012).
10. R. Takasu, K. Sekine, and T. Takamura, *Journal of power sources*, **81** 224-228 (1999).

11. I.-M. Hsing, X. Wang, and Y.-J. Leng, *Journal of the Electrochemical Society,* **149** (5), A615 (2002).
12. C. Huang, S. Zhuang, and F. Tu, *Journal of the Electrochemical Society,* **160** (2), A376 (2012).
13. Y. Hoshi, Y. Narita, K. Honda, T. Ohtaki, I. Shitanda, and M. Itagaki, *Journal of Power Sources,* **288** 168-175 (2015).
14. T. F. Landinger, G. Schwarzberger, and A. Jossen, *Journal of Power Sources,* **488** 229463 (2021).
15. C.-H. Kim, S.-I. Pyun, and J.-H. Kim, *Electrochimica Acta,* **48** (23), 3455-3463 (2003).
16. V. J. Ovejas and A. Cuadras, *Batteries,* **4** (3), 43 (2018).
17. F. Kenji, K. Kazuhiko, I. Kennichi, and Y. Masaki, *Journal of Power Sources,* **69** (1), 165-168 (1997).
18. S. Zhang and P. Shi, *Electrochimica Acta,* **49** (9), 1475-1482 (2004).
19. D. Chen, S. Sun, G. Yu, L. Qin, W. Wang, M. Jiang, and J. Chen, *Carbon,* **166** 91-100 (2020).
20. M. Itagaki, K. Honda, Y. Hoshi, and I. Shitanda, *Journal of Electroanalytical Chemistry,* **737** 78-84 (2015).
21. J. J. Giner-Sanz, E. Ortega, and V. Pérez-Herranz, *Electrochimica Acta,* **209** 254-268 (2016).
22. B. A. Boukamp, *tm-Technisches Messen,* **71** (9), 454-459 (2004).
23. A. Bardos, R. N. Zare, and K. Markides, *Chemical physics letters,* **402** (1-3), 274-278 (2005).
24. A. Chandra and B. Bagchi, *The Journal of chemical physics,* **110** (20), 10024-10034 (1999).
25. S. Sridharan, J. McCammon, and J. Hubbard, *The Journal of chemical physics,* **90** (1), 237-240 (1989).
26. I. A. J. Gordon, S. Grugeon, H. Takenouti, B. Tribollet, M. Armand, C. Davoisne, A. Débart, and S. Laruelle, *Electrochimica Acta,* **223** 63-73 (2017).
27. D. Pritzl, J. Landesfeind, S. Solchenbach, and H. A. Gasteiger, *Journal of The Electrochemical Society,* **165** (10), A2145-A2153 (2018).